Available online at www.sciencedirect.com

SciVerse ScienceDirect

Journal of the European Ceramic Society 32 (2012) 2283–2292

www.elsevier.com/locate/jeurceramsoc

The role of K_2O on sintering and crystallization of glass powder compacts in the Li_2O–K_2O–Al_2O_3–SiO_2 system

Hugo R. Fernandes [a,*], Dilshat U. Tulyaganov [a,b], Maria J. Pascual [c], Vladislav V. Kharton [a], Aleksey A. Yaremchenko [a], José M.F. Ferreira [a]

[a] *Department of Ceramics and Glass Engineering, University of Aveiro, CICECO, 3810-193 Aveiro, Portugal*
[b] *Turin Polytechnic University in Tashkent, 17, Niyazova str., 100174 Tashkent, Uzbekistan*
[c] *Instituto de Cerámica y Vidrio (CSIC), C/Kelsen 5, Campus de Cantoblanco, 28049 Madrid, Spain*

Received 2 August 2011; received in revised form 18 January 2012; accepted 6 February 2012
Available online 3 March 2012

Abstract

The effects of K_2O content on sintering and crystallization of glass powder compacts in the Li_2O–K_2O–Al_2O_3–SiO_2 system were investigated. Glasses featuring SiO_2/Li_2O molar ratios of 2.69–3.13, far beyond the lithium disilicate (LD-$Li_2Si_2O_5$) stoichiometry, were produced by conventional melt-quenching technique. The sintering and crystallization behaviour of glass powders was explored using hot stage microscopy (HSM), scanning electron microscopy (SEM), differential thermal (DTA) and X-ray diffraction (XRD) analyses. Increasing K_2O content at the expense of SiO_2 was shown to lower the temperature of maximum shrinkage, eventually resulting in early densification of the glass-powder compacts. Lithium metasilicate was the main crystalline phase formed upon heat treating the glass powders with higher amounts of K_2O. In contrast, lithium disilicate predominantly crystallized from the compositions with lower K_2O contents resulting in strong glass–ceramics with high chemical and electrical resistance. The total content of K_2O should be kept below 4.63 mol% for obtaining LD-based glass–ceramics.

Keywords: Glass–ceramics; Lithium disilicate; Sintering; Thermo-physical properties

1. Introduction

Sintering of glass-powder compacts is a common processing route for obtaining glass–ceramic (GC) materials with desired properties.[1,2] The glass powders with high specific surface area intrinsically provide uniformly distributed nucleus sites in the entire volume of the glass.[3–7] The properties of GCs are determined by crystalline phases precipitated from the glass reservoir whilst an excessively high crystal growth rate is to be avoided to not develop coarse microstructure limiting achievement of high mechanical strength.[1,8–10] Additionally, sintering should preferably take place prior crystallization thus both events being independent processes.

Lithium disilicate GCs have attracted much interest due to a wide range of practical applications such as ceramic composites, ceramic–metal sealing, and dental restoration[11–13]. Production of those materials might be alternatively based on sintering and crystallization of glass powder compacts. In particular, dentistry restoration systems IPS Empress® 2 for restoring three-unit fixed partial dentures up to the second premolar have so far been prepared by hot-pressing technology of sintered ingots.[14] Apparently, besides the practical aspects, lithium disilicate glasses have been a subject of many nucleation and crystallization theories for decades.[15–18] These studies focused on the Li_2O–SiO_2 binary glass system and discussed the growth interrelation between the $Li_2Si_2O_5$ and Li_2SiO_3 (lithium metasilicate) crystalline phases.[15–20]

In our previous attempts, the glasses containing Al_2O_3 and K_2O and featuring SiO_2/Li_2O molar ratios (3.13–4.88) were produced by conventional melt-quenching technique along with a bicomponent glass $23Li_2O$–$77SiO_2$ (mol%).[19,20] Sintering and

* Corresponding author. Tel.: +351 234 370217; fax: +351 234 425300.
E-mail address: h.r.fernandes@ua.pt (H.R. Fernandes).

0955-2219/$ – see front matter © 2012 Elsevier Ltd. All rights reserved.
doi:10.1016/j.jeurceramsoc.2012.02.003

crystallization studies of glass powder compacts revealed that $23Li_2O–77SiO_2$ composition exhibited high fragility along with low flexural strength and density. Addition of Al_2O_3 and K_2O in equimolar amount to $Li_2O–SiO_2$ compositions resulted in improved densification and mechanical strength.[19]

Recently we attempted to synthesis glasses in the glass forming region of $Li_2O–K_2O–Al_2O_3–SiO_2$ system with SiO_2/Li_2O molar ratios varying between 2.69 and 3.13.[21] The role of K_2O and K_2O/SiO_2 ratios on structural transformations, properties of new glasses in bulk form along with their crystallization mechanism was investigated. The ^{29}Si MAS-NMR spectra evidenced a mixture of Q^4 (Si) and Q^3 (Si) as the predominant structural units in all the glasses. Moreover, upon increasing K_2O content new Q^2 groups appeared, the amount of Q^3 units increased, whereas Q^4 diminished, suggesting depolymerisation of the silicate glass network. The addition of K_2O was found to promote surface crystallization in glasses, as well as the predominant formation of lithium metasilicate phase.

This work, as the logical continuation of the recent study,[21] aims at investigating the effects of K_2O on sintering and crystallization of glass powder compacts in the $Li_2O–K_2O–Al_2O_3–SiO_2$ system. The same glass compositions with SiO_2/Li_2O molar ratios varying between 2.69 and 3.13 have been prepared but in the frit form, and the sintering and crystallization of glass-powder compacts were analysed by hot stage microscopy (HSM), scanning electron microscopy (SEM), differential thermal (DTA) and X-ray diffraction (XRD) analyses. Another objective was to determine the influence of K_2O contents and K_2O/SiO_2 ratios on thermal, mechanical and electrical properties of resultant glass–ceramic materials.

2. Experimental procedure

2.1. Glass preparation

A total of 8 compositions were prepared according to the general formulae $23.7\ (71.78-x)\ SiO_2{\cdot}2.63\ Al_2O_3{\cdot}(2.63+x)\ K_2O{\cdot}23.7\ Li_2O$, where x changed from 0 to 10.[21] Accordingly, the glasses have been labelled as GK_x depending on the amount of K_2O being substituted for SiO_2 in the glass compositions. For example: GK_0 corresponds to the parent composition, i.e., $x=0$ and $K_2O/Al_2O_3=1$. Table 1 presents the detailed compositions of the glasses along with their corresponding SiO_2/Li_2O, SiO_2/K_2O and K_2O/Al_2O_3 ratios.

Table 1
Compositions of the experimental glasses.

	Oxides (mol%)						
	Li_2O	K_2O	Al_2O_3	SiO_2	SiO_2/Li_2O	SiO_2/K_2O	K_2O/Al_2O_3
GK	22.96	2.63	2.63	71.78	3.13	27.29	1.00
$GK_{0.5}$	22.96	3.13	2.63	71.28	3.10	22.77	1.19
GK_1	22.96	3.63	2.63	70.78	3.08	19.50	1.38
$GK_{1.5}$	22.96	4.13	2.63	70.28	3.06	17.02	1.57
GK_2	22.96	4.63	2.63	69.78	3.04	15.07	1.76
$GK_{2.5}$	22.96	5.13	2.63	69.28	3.02	13.50	1.95
GK_5	22.96	7.63	2.63	66.78	2.91	8.75	2.90
GK_{10}	22.96	12.63	2.63	61.78	2.69	4.89	4.80

Powders of technical grade SiO_2 (purity > 99.5%) and of reactive grade Al_2O_3, Li_2CO_3, and K_2CO_3 were used. Homogeneous mixtures of batches (~100 g) obtained by ball milling were calcined at 800 °C for 1 h, melted in Pt crucibles at 1550 °C for 1 h in air and then quenched in cold water. The obtained frits were dried and milled in a high-speed agate mill. The mean particle size of the glass powders as determined by light scattering technique (Beckman Coulter LS 230, CA, USA; Fraunhofer optical model) was about 5–10 μm.

2.2. Sintering and crystallization of glass powder compacts

A side-view hot-stage microscope (HSM, Leitz Wetzlar, Germany) equipped with a Pixera video-camera and image analysis system was used to investigate the sintering behaviour of glass powder compacts. The cylindrical shaped samples from glass powder compacts with height and diameter of ≈3 mm were prepared by cold-pressing the glass powders. The cylindrical samples were placed on a 10 mm × 15 mm × 1 mm alumina (>99.5 wt.% Al_2O_3) support and the measurements were conducted in air with a heating rate (β) of 5 K/min. The temperature was measured with a chromel–alumel thermocouple contacted under the alumina support. The temperatures corresponding to the characteristic viscosity points [first shrinkage (T_{FS}), maximum shrinkage (T_{MS}), softening (T_D), half ball (T_{HB}) and flow (T_F)] were obtained from the graphs and photomicrographs taken during the hot-stage microscopy experiment.[22,23]

Apart from HSM investigation, the sintering process was explored using non-isothermal heat treatment of glass-powder compacts. Rectangular bars (4 mm × 5 mm × 50 mm) prepared by uniaxial pressing (80 MPa) were sintered at 800, 850 and 900 °C for 1 h. A heating rate of 2 K/min was maintained in order to prevent deformation of the samples.

The following characterization techniques were employed to analyse sintered materials: (1) Archimedes' method (i.e. immersion in diethyl phthalate) to measure the apparent density; (2) dilatometry measurements (Bahr Thermo Analyze DIL 801 L, Hüllhorst, Germany; heating rate 5 K/min) to measure coefficient of thermal expansion (CTE) (standard deviation obtained from 3 samples was $\pm 0.1 \times 10^{-6}$/K); (3) differential thermal analysis in air (DTA, Labsys setaram TG-DTA; heating rate 5 and 10 K/min); (4) 3-point bending strength tests were performed on rectified parallelepiped bars of sintered GCs (Shimadzu Autograph AG 25 TA, 0.5 mm/min displacement): the results were obtained from 10 different independent samples; (5) chemical resistance was established according to ISO test standards, i.e. immersing the materials in acetic acid at 80 °C for 16 h and evaluating possible weight loss ($\mu g/cm^2$)[24]; (6) crystalline phases were identified by X-ray diffraction analysis (Rigaku Geigerflex D/Mac, C Series, Japan; Cu K_a radiation, $2\theta = 10–60°$ with a 2θ-step of 0.02°/s) comparing the experimental X-ray patterns to standards compiled by the international centre for diffraction data (ICDD); and (7) microstructure observations were done on polished (mirror finishing) and then etched samples (immersion in 2 vol.% HF solution for 2 min) by field

emission scanning electron microscopy (FE-SEM, Hitachi S-4100, Japan, 25 kV acceleration voltage, beam current 10 μA) under secondary electron mode.

For the measurements of total conductivity, dense ceramic samples sintered at 900 °C were cut into disks with thickness of 1–3 mm (diameter of 14 mm) and then polished with diamond pastes. Porous Ag electrodes were applied onto both sides of the glass–ceramic disks and sintered at 600 °C for 5–10 min. The total conductivity (σ) was determined by alternating current (AC) impedance spectroscopy using a HP4284A precision LCR meter in the frequency range 20 Hz to 1 MHz. The measurements were performed at 630–800 K in flowing dry and wet air or argon, where the water vapour partial pressure was continuously monitored by a Jumo humidity transducer. The lower temperature limit was associated with increasing electrical resistance of the glass–ceramics on cooling, leading to a higher noise level and lower accuracy; the upper limit was selected in order to avoid possible volatilization of the alkaline metal oxide components. The gas flows were dried by passing through silica gel or humidified by bubbling through water at room temperature.

3. Results

3.1. Glass and glass–ceramic samples preparation

Heating at 1550 °C for 1 h was adequate to obtain amorphous frits from all the investigated compositions as confirmed by the absence of crystalline inclusions using XRD analysis. Apparently, glass preparation temperature decreases with growing K_2O content. Dense samples of rectangular shape were obtained after sintering of glass-powder compacts at 800, 850 and 900 °C for 1 h. However, GK_5 and GK_{10} exhibited clear signs of softening at temperature ≥800 °C (Fig. 1) due to their higher contents of alkaline oxides ($Li_2O + K_2O$).[25–29]

3.2. Sintering process of glass-powder compacts

During sintering of a glass-powder compact, smaller particles get sintered first and sintering kinetics at the first shrinkage is dominated by the neck formation amongst smallest particles via viscous flow.[30,31] Maximum shrinkage is reached when larger pores have disappeared due to viscous flow that reduces their radii with time.[32] However, some processes, e.g. crystallization, occurring at the very end of sintering process might affect the densification kinetics. A comparison between DTA and HSM results under the same heating conditions can be useful to investigate the effect of glass composition on sintering and devitrification phenomena. In general, two different trends related to the sintering and crystallization behaviour of the glasses can be observed[33]: (1) the beginning of crystallization (T_c) occurs after the final sintering stage and, thus, sintering and crystallization are independent processes; and (2) T_c appears before the maximum density has been reached, and the crystallization process starts before complete densification, thus, preventing further sintering.

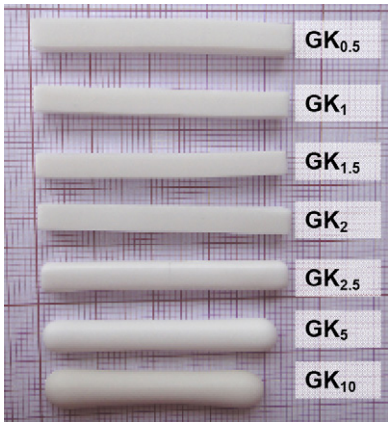

Fig. 1. Appearance of glass powder compact bars after sintering at 900 °C for 1 h.

There are several important characteristic viscosity points based on the relation between the temperatures measured by HSM and corresponding viscosities[22,34]: (1) first shrinkage (T_{FS}): the temperature at which the pressed sample starts to shrink, log $\eta = 9.1 \pm 0.1$, where η is the viscosity in dPa s; (2) point of maximum shrinkage (T_{MS}): the temperature at which maximum shrinkage of the glass-powder compact is achieved before it starts to soften, log $\eta = 7.8 \pm 0.1$; (3) softening point (T_D): the temperature at which the first signs of softening are observed which is generally shown by the disappearance or rounding of the small protrusions at the edges of the sample, log $\eta = 6.3 \pm 0.1$; (4) half ball point (T_{HB}): the temperature at which the section of the observed sample forms a semicircle on the microscope grid, log $\eta = 4.1 \pm 0.1$, and (5) flow point (T_F): the temperature at which the maximum height of the drop of the molten glass corresponds to a unit on the microscopic scale, log $\eta = 3.4 \pm 0.1$. A/A_0 corresponds to the ratio of final area/initial area of the glass-powder compacts.

The variation in the relative area (A/A_0) and heat flow with respect to temperature is shown in Fig. 2, revealing two steps of sintering. The thermal characteristics and sintering parameters of glasses obtained by means of DTA and HSM are summarized in Table 2. The initiation of sintering occurred at ~484–491 °C (T_{FS1}) in all compositions whilst the extent of densification at the first stage (i.e. temperature interval between T_{MS1} and T_{FS1}) significantly decreased with increasing K_2O content and K_2O/SiO_2 ratio. The first sintering stage ended at the point of first maximum shrinkage (T_{MS1}) that was fairly close to the onset of crystallization temperature (T_c).

The second stage of densification occurred in competition with devitrification process (Fig. 2) that subsequently might cause a viscosity increase.[33] However, the viscosity did not rise in such an extent to prevent sintering.[19] In contrast, shrinkage values (Δ_2) of GK_0–GK_2 glasses were comparable with relevant data obtained at the first stage. The subsequent GK_5–GK_{10} compositions exhibited highest values of shrinkage suggesting that the densification processes for these glasses mostly occurred during the second sintering stage. Another feature was that the temperature of second shrinkage (T_{FS2}) and the corresponding point of maximum shrinkage (T_{MS2}) decreased with increasing amounts of K_2O.

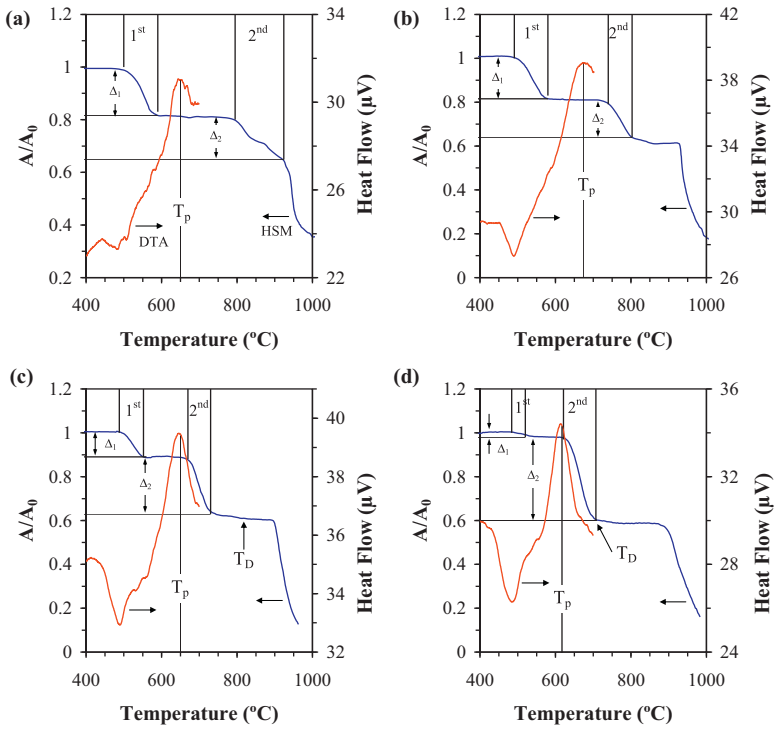

Fig. 2. DTA and HSM curves for glass-powders (a) GK_0, (b) GK_2, (c) GK_5, and (d) GK_{10}.

Table 2
Thermal characteristics of glasses and their sintering parameters.

x	DTA			HSM									
	T_g (°C)	T_c (°C)	T_p (°C)	T_{FS1}(°C)	T_{MS1}(°C)	Δ_1	T_{FS2} (°C)	T_{MS2} (°C)	Δ_2	A/A_0	T_D (°C)	T_{HB} (°C)	T_F (°C)
0	507	599	672	487	611	0.18	774	924	0.17	0.65	929	945	964
1	499	596	669	491	611	0.18	758	874	0.20	0.62	947	957	967
2	494	588	675	487	593	0.19	717	870	0.20	0.61	928	937	954
5	493	563	651	488	565	0.11	658	821	0.28	0.61	830	910	929
10	490	559	616	484	541	0.02	621	707	0.39	0.59	709	916	939

The photomicrographs demonstrating a change in the geometrical shape with temperature, as obtained from HSM, are presented in Fig. 3. The value of T_D for GK_0 is about 929 °C, which is higher than the maximum sintering temperature used in the experimental procedure (900 °C). Therefore no deformation sighs in GK_0 samples were revealed (Fig. 1), likewise for GK_1 and GK_2 that exhibited T_D values at about 947 °C and 928 °C, respectively (Table 2). Compositions with higher added amounts of K_2O exhibited lower ability to withstand the same temperature range. For instance, compositions GK_5 and GK_{10} reached T_D at 830 and 709 °C, T_{HB} at 910 and 916 °C, and T_F at 929 and 939 °C, respectively (Table 2).

Fig. 3. HSM images of glass powder compacts on alumina substrates (*corresponds to T_D of composition GK_0).

3.3. Phase assemblage and microstructure

Fig. 4 presents the X-ray diffractograms of glass powder compacts after heating at 800, 850 and 900 °C for 1 h. Lithium metasilicate is the major phase whilst quartz and lithium disilicate are minor phases in GK_0 at 800 °C. Low intensive peaks of lithium disilicate also appeared in the $GK_{0.5}$–GK_2 samples heat treated at this temperature. Increasing the heat treatment temperature to 850–900 °C favoured formation of lithium disilicate in detriment of lithium metasilicate within the x range of 0–2. However, the intensity of lithium disilicate peaks decayed with increasing K_2O contents and the observed results suggest that the total amount of K_2O in a glass should be less than 4.63 mol% (or x should vary in the range of 0–2) to obtain lithium disilicate as the predominate crystalline phase. Thus, lithium metasilicate was the only crystalline phase formed in the glasses containing higher amounts of K_2O after sintering at 800, 850 and 900 °C (in GK_5 weak peaks of orthoclase were also identified).

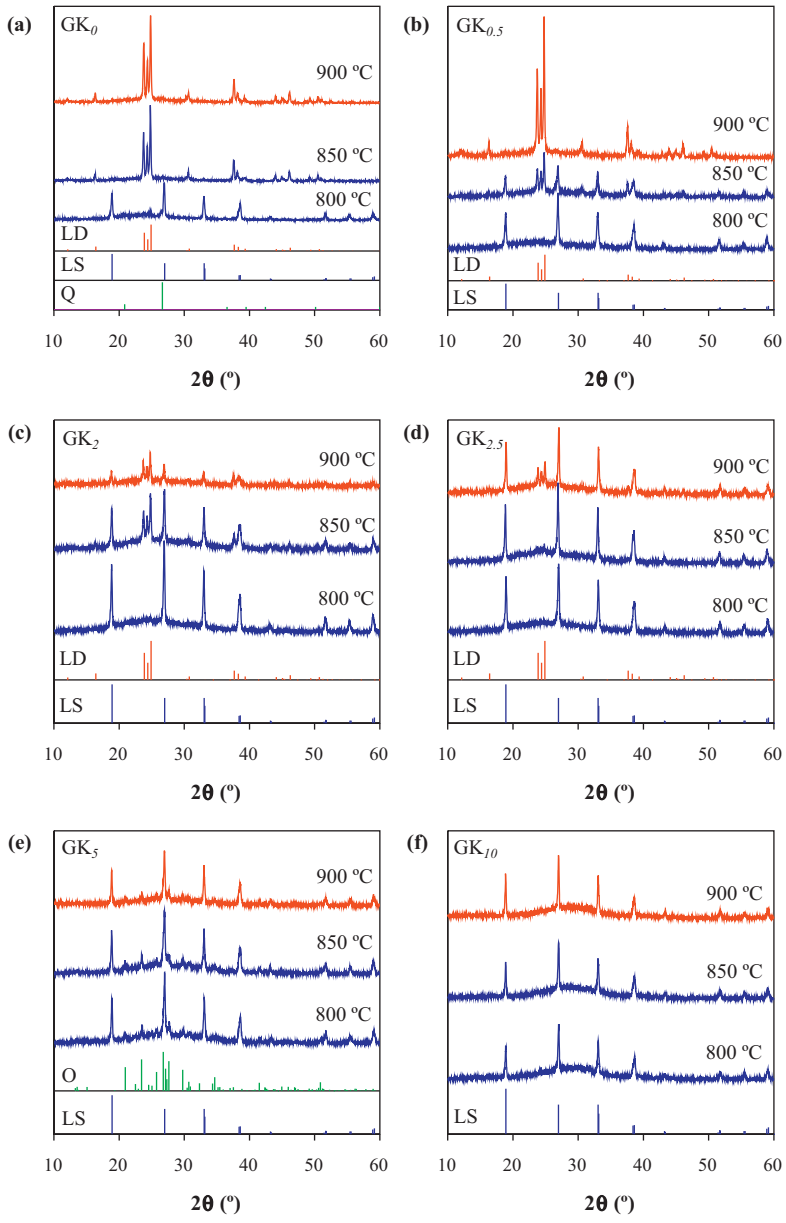

Fig. 4. X-ray diffractograms of glass powder compacts after heat treatment at different temperatures for 1 h: (a) GK_0, (b) $GK_{0.5}$, (c) GK_2, (d) $GK_{2.5}$, (e) GK_5, and (f) GK_{10}. LS: lithium silicate (Li_2SiO_3, ICCD card 01-029-0828); LD: lithium disilicate ($Li_2Si_2O_5$, ICCD card 01-070-4856); Q: quartz (SiO_2, ICCD card 01-077-1060); O: orthoclase ($K_4Al_4Si_{12}O_{32}$, ICCD card 01-080-2108).

Fig. 5 presents the SEM images of glass powder compacts of compositions GK_0, $GK_{2.5}$ and GK_5 after heat treatment at 800, 850 and 900 °C for 1 h. The microstructure of parent composition GK_0 heat treated at 800 °C (Fig. 5a) reveals the occurrence of dendritic crystal growth of lithium metasilicate and small crystals of quartz dispersed in the matrix, which are in accordance with the results obtained by XRD (Fig. 4a). It is known that lithium metasilicate crystals are particularly easy to dissolve from GC by diluted hydrofluoric acid (HF) whilst the surrounding aluminosilicate glassy matrix is considerably more resistant to acid attack.[1] Thus, its presence is recognized by the replica image resultant from acid etching. At 850 °C the microstructure changed drastically revealing the presence of laminar fibres of lithium disilicate embedded in the glass matrix which further grew with temperature increasing to 900 °C. With increasing added amounts of K_2O the content of glassy phase increased and lithium metasilicate appeared as the predominant crystalline phase, being in good agreement with the XRD results presented in Fig. 4. In the case of $GK_{2.5}$ composition, the presence of laminar lithium disilicate crystals is only apparent in the micrograph of the sample heat treated at 900 °C (Fig. 5d), although traces of lithium disilicate have been detected at 850 °C (Fig. 4d). The micrographs of GK_5 composition (Fig. 5h–j) are dominated by the morphological features of lithium metasilicate crystals that underwent extensive dissolution by HF attack. The small orthoclase content detected by XRD is also apparent as small equiaxed and whiter crystals.

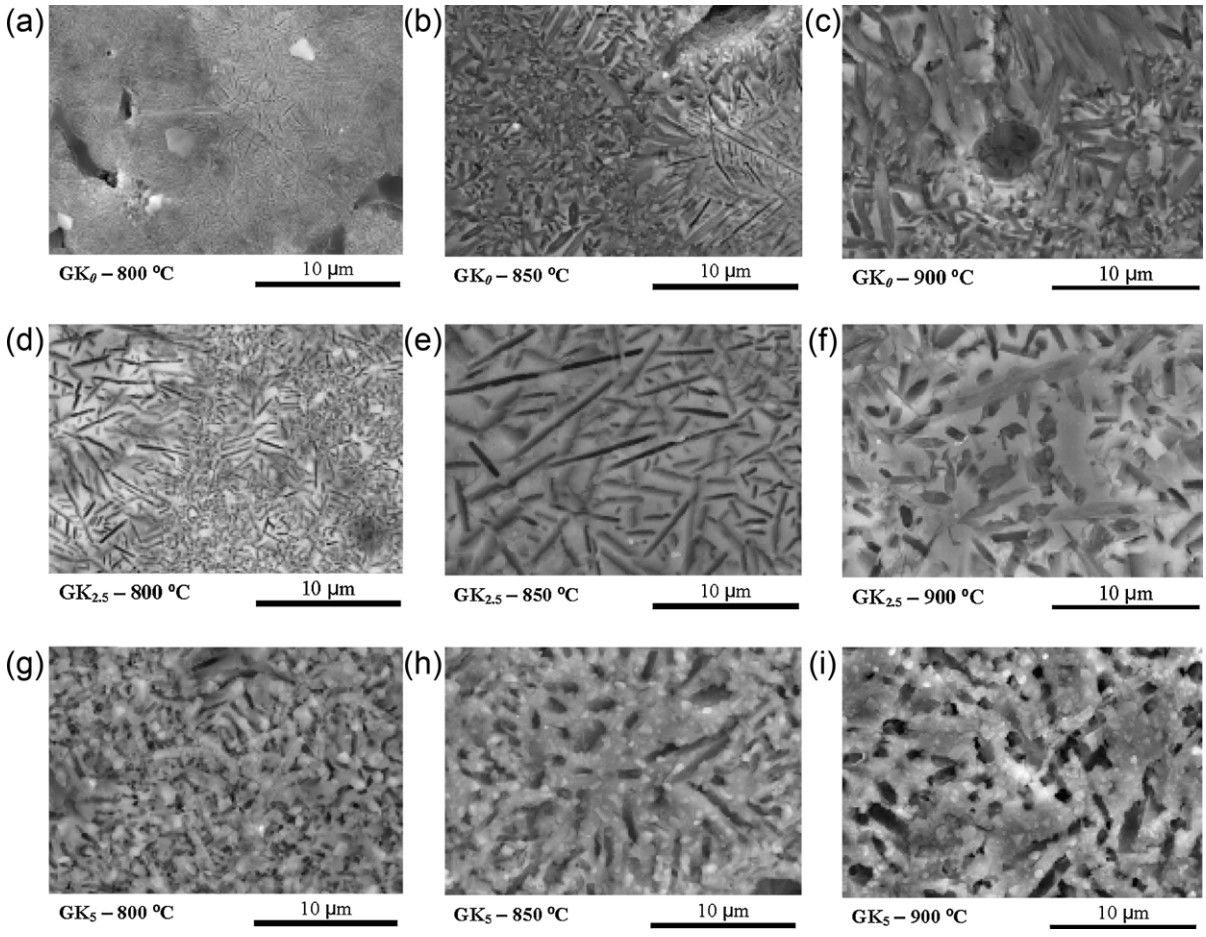

Fig. 5. SEM images of glass powder compacts heat treated at different temperatures for 1 h.

3.4. Density, bending strength, CTE and chemical resistance of glass-powder compacts

Table 3 presents density and bending strength values of glass powder compacts heat treated at 800, 850 and 900 °C for 1 h. The glass–ceramics GK_0–GK_2 exhibited maximum density (2.34–2.38 g/cm^3) and bending strength (~173–224 MPa) after heat treatment at 900 °C. The samples $GK_{2.5}$, GK_5 and GK_{10} having higher K_2O/SiO_2 ratios possessed maximum density (2.34–2.38 g/cm^3) and bending strength values (~89–148 MPa) at the lower temperatures (800 and 850 °C) that are in accordance with the results of HSM and DTA.

The superior mechanical properties of GK_0–GK_2 glass–ceramic samples can be explained by the formation of lithium disilicate crystals (Fig. 5) and their higher contribution to mechanical resistance in comparison to lithium metasilicate.[35,36]

Fig. 6 shows the evolution CTE and chemical durability with respect to K_2O content for glass powder compacts heat treated at 900 °C for 1 h. The chemical resistance of GCs is high for small x values but noticeably decreased with increasing K_2O/SiO_2 ratios. This trend was more than expected considering the relatively high solubility of lithium metasilicate in acidic environment.[1] The increasing amounts of residual glassy phase for samples with $x > 2.5$, as deduced from the noisy backgrounds in Fig. 4, will also negatively affect the chemical stability of glass–ceramics.[37]

The change of CTE with respect to K_2O shows almost a linear trend (Fig. 6). In particular, CTE gradually increases with the increments of K_2O in glass–ceramics. Since a GC might be considered as a composite material, its CTE depends on the type and volume fraction of both crystalline and glassy phases.[38–40] The increase of CTE with the increments of K_2O can be explained by the concomitant increase in the volume fraction of glassy phase (Fig. 4), and by the precipitation of lithium metasilicate and orthoclase phases.[41]

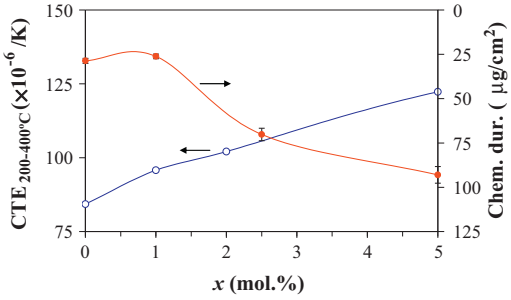

Fig. 6. Evolution of $CTE_{200–400\ °C}$ and chemical durability with the amount of K_2O for glass powder compacts heat treated at 900 °C for 1 h.

Table 3
Properties of the glass powder compacts heat treated at several temperatures in air during 1 h.

	x (mol%)					
	0	0.5	1.5	2.5	5	10
Density (g/cm^3)						
800 °C	2.19 ± 0.03	2.25 ± 0.02	2.35 ± 0.01	2.34 ± 0.03	2.36 ± 0.01	2.38 ± 0.01
850 °C	2.25 ± 0.03	2.36 ± 0.03	2.35 ± 0.03	2.31 ± 0.03	2.35 ± 0.03	2.30 ± 0.03
900 °C	2.36 ± 0.03	2.38 ± 0.03	2.35 ± 0.03	2.28 ± 0.03	2.28 ± 0.03	2.22 ± 0.03
Bending strength (MPa)						
800 °C	81 ± 8	88 ± 19	125 ± 6	148 ± 9	126 ± 4	89 ± 8
850 °C	216 ± 3	151 ± 11	176 ± 11	138 ± 10	139 ± 12	76 ± 10
900 °C	224 ± 4	173 ± 8	205 ± 13	107 ± 12	79 ± 6	–

3.5. Electrical properties

Typical examples of the impedance spectra of glass–ceramic disks with porous Ag electrodes are presented in Fig. 7. In all cases, the spectra consist of one semicircle with a small electrode tail in the low-frequency range. In general, this form is characteristic of dielectric materials, in agreement with high values of the electrical resistance which can be calculated from low-frequency intercept of the semicircles on the real axis.

The total conductivity (Fig. 8) follows Arrhenius dependence and tends to moderately decrease in the high-temperature range with incremental amounts of K_2O. The latter trend originates from decreasing activation energy (E_a) when K_2O content increases. Fig. 9 displays the activation energy values calculated by the Arrhenius equation:

$$\sigma = \frac{A_0}{T} \exp\left(\frac{E_a}{RT}\right)$$

were A_0 is the pre-exponential factor. Although the observed variations of both σ and E_a are relatively minor at K_2O concentrations varying in the narrow range of 2.63–7.63 mol%, these are higher than instrumental and statistical errors. Attempts to determine the type of prevailing charge carriers using concentration cells, where the dense glass–ceramic disks are placed under

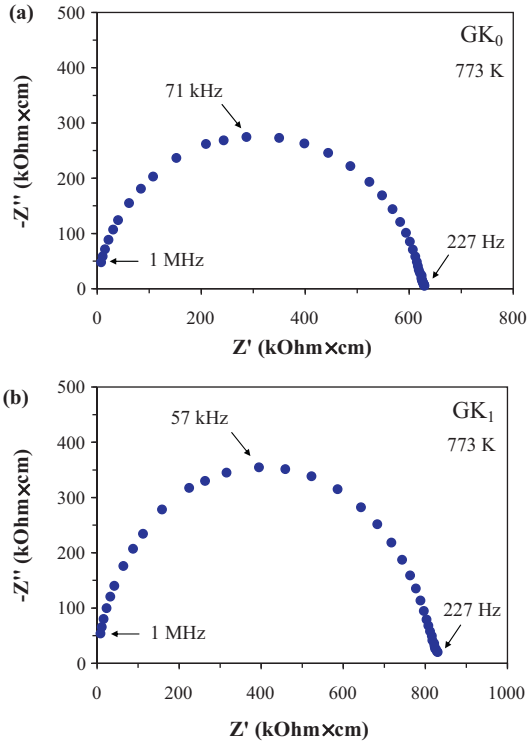

Fig. 7. Examples of impedance spectra of the glass–ceramics with Ag electrodes, in dry air: (a) GK_0 and (b) GK_1.

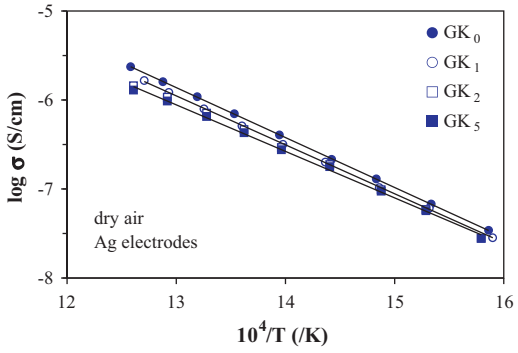

Fig. 8. Temperature dependence of the total conductivity of glass–ceramic materials in dry air.

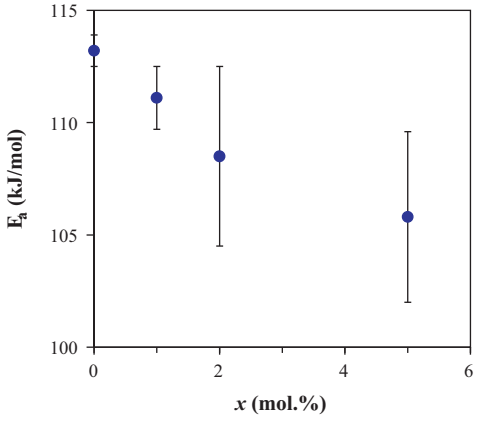

Fig. 9. Composition dependence of the activation energy for total conductivity of the glass–ceramic materials in dry air.

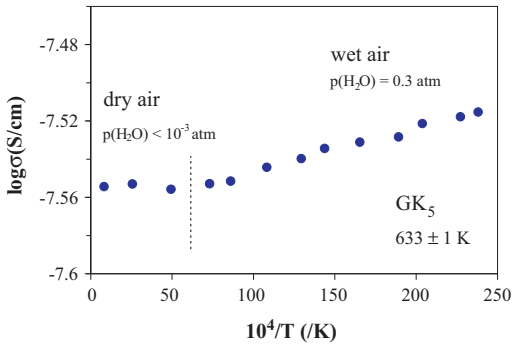

Fig. 10. Time dependence of the total conductivity of GK_5 glass–ceramics in dry and wet air.

oxygen, water vapour and lithium chemical potential gradient, failed due to the very high resistivity of the studied materials. Nonetheless, the tendency to lowering the conductivity activation energy with K_2O additions may indicate a significant ionic contribution to transport processes. In the latter case, the ionic charge carriers may include either metal cations (Li^+, K^+) or protons formed due to water incorporation, promoted by potassium doping. Indeed, the total conductivity of the glass–ceramics was found essentially independent on the oxygen partial pressure, varied from 0.21 atm (dry air) down to approximately 10^{-5} atm (flowing argon). At the same time, increasing humidity at 633 K resulted in a slow increase of the conductivity (Fig. 10). Again, this effect is small but significant with respect to the experimental error (2–3%). Notice also that keeping of the glass–ceramics in humid atmospheres at 300–400 K during 2 weeks did not lead to any significant changes in their bulk conductivity, thus suggesting that minor hydration is only observed at elevated temperatures, probably due to kinetic reasons.

Whatever the microscopic mechanisms, the glass–ceramic materials exhibit excellent insulating properties at low temperatures. The estimates of their total conductivity at room temperature, obtained by extrapolation of the Arrhenius dependencies, vary from 2×10^{-18} S/cm (GK_0) to 1×10^{-17} S/cm (GK_5). Regardless of the slight decrease in the electrical resistivity induced by K_2O doping, the overall resistance level is very high.

4. Discussion

From the results of our recent study[21] the addition of K_2O at the expense of SiO_2 in the Li_2O–K_2O–Al_2O_3–SiO_2 system was found to promote surface crystallization in bulk glasses, as well as the predominant formation of lithium metasilicate phase. However, considering that the production of lithium disilicate GCs for most of the intended applications involves the sintering and crystallization of glass powder compacts, it is of paramount importance to evaluate how these thermal events are affected by the composition. Therefore, the current work is focused on studying the influence of K_2O amount and K_2O/SiO_2 ratio on sintering/crystallization behaviour of glass powder compacts.

Glasses have been produced at 1550 °C for 1 h to escape any signs of nonhomogeneity in the form of crystalline inclusions. Volatilization of chemical species should be very low. As a matter of fact, analogous glasses from the SiO_2–Li_2O–Al_2O_3–K_2O–ZrO_2–P_2O_5 system that were firstly melted at 1370 °C for 2 h and subsequently heat treated at 1500 °C for 1.5 h demonstrated to have almost the same chemical compositions after analysis as the planed starting compositions.[42]

Densification of glass powder compacts is obtained through viscous flow at temperatures slightly higher than the glass transition temperature (T_g). The desired order of events in a glass-powder sintering process occurs when the sintering process is completed before crystallization begins. Under these conditions, dense materials are obtained.[33] From HSM and DTA data it can be concluded that increasing K_2O/SiO_2 ratio led to diminishing of T_{FS1}, T_{MS1}, T_{FS2} and T_{MS2} parameters and temperature intervals between T_{MS} and T_{FS} at both the first and the second sintering stages. Consequently, K_2O-richer samples get sintered during shorter temperature interval and at lower temperatures than compositions with lower K_2O contents. Therefore, the GK_5 and GK_{10} compositions reached half ball point (T_{HB}) even earlier than softening point (T_D) was attained in GK_0–GK_2 glasses (Table 2 and Fig. 3). This behaviour is in a good correlation with the trend observed in the ^{29}Si NMR spectra of corresponding glasses pointing towards depolymerisation of the silicate glass network when K_2O/SiO_2 ratio increased.[21]

In general, the sintering and crystallization events occurring in the experimental compositions appear as independent processes only during the first sintering stage. Although these compositions did not strictly follow the desired sequence of events and sintering was partially impeded by crystallization, all glass-powder compacts demonstrated excellent sintering ability and achieved the maximum expected density ($A/A_0 \sim 0.6$).[33] Similar trends were observed in our previous work where sintering and devitrification processes were investigated in Li_2O–SiO_2 compositions with equimolar additions of Al_2O_3 and K_2O.[19]

Additionally, the difference between T_c and T_g must be also taken into account. From the Table 2 this difference is about 92–97 °C for GK_0–GK_2 glasses and 69–70 °C for GK_5–GK_{10} glasses confirming that compositions with lower K_2O contents show smaller tendency to crystallization and greater glass stability.

XRD and SEM results demonstrated that K_2O content plays a crucial role in the crystallization process of glass-powder compacts. As a matter of fact, the trend for the preferential crystallization of lithium metasilicate with increasing potassium content resemble data received from crystallization of relevant bulk glasses.[21] Using the model proposed by Bischoff et al.[36] and ^{29}Si MAS-NMR results from our previous work[21] we can attempt explaining the effect of suppressing the crystallization of $Li_2Si_2O_5$ and promoting the formation of Li_2SiO_3 with increasing K_2O contents. In particular, considering significant decrease of Q^4 groupings in K_2O-rich glasses (e.g. GK_5 and GK_{10}), the feasibility of the reaction Q^4 (glass) + Q^2 (cryst.) ↔ 2 Q^3 (cryst.) diminishes considerably. This leads to the formation of single phase Li_2SiO_3 directly from Q^2 or via reaction 2 Q^3 (glass) ↔ Q^2 (cryst.) + Q^4 (glass).[36]

Another interesting aspect is that the glass powder compacts are more prone to the formation of lithium disilicate for $x \leq 2$, than the corresponding bulk glasses where $x \leq 1$. This behaviour can be ascribed to the difference in preparation routes of the parent glasses as water quenching of the glass increases the OH^- content. The hydroxyl groups may act as a modifier and break the silicate network, thus, reducing the viscosity and activation energy of viscous flow.[19]

Sintered glass powder compacts with K_2O content less than 4.64 mol% featured enhanced mechanical properties (bending strength ~173–224 MPa) and high chemical resistance (~25–50 μg/cm^2) due to the predominant crystallization of lithium disilicate crystalline phase. The chemical durability of the experimental compositions is similar to that reported for IPS Empress® 2 (50 μg/cm^2), but materials are more resistant than IPS Empress® 1 (122 mg/cm^2) for layering technique.[1]

The 3-point bending strength values are lower than those reported for IPS Empress® 2 (400 ± 40 MPa).[1,43] It is known, however, that hot pressing technique used to prepare samples of commercial GC can significantly improves bending strength.[1] To prove this assumption, additional experiments were attempted on the synthesis and processing of a commercial glass–ceramic composition: 69.6 SiO_2, 1.10 Al_2O_3, 3.90 P_2O_5, 3.30 K_2O, 15.4 Li_2O, 0.50 TiO_2, 0.30 CeO_2, 0.30 La_2O_3, 5.20 ZnO, 0.20 MgO, 0.20 Fe_2O_3 (wt.%).[43] A bending strength of 341 ± 98 MPa was reported for this material when processed by hot pressing.[43] According to the specifications given,[43] the glass was melted in a platinum crucible at 1550 °C for 1 h followed by quenching in water, drying and milling the frit to an average particle size of 20–30 μm. Then, rectangular bars (4 mm × 5 mm × 50 mm) were prepared by uniaxial pressing (80 MPa) following the same experimental procedure used for compositions GK_0–GK_{10}. The as obtained bars were also similarly fired at 500 °C for 1 h and then at 850 °C for 2 h (the rate of heating was 30 K/min) as recommended in.[43] Thus, hot pressing procedure has been excluded from sample preparation. The average flexural strength (for 10 samples) measured in a testing machine (Shimadzu Autograph AG 25 TA) was 199 ± 14 MPa, which is comparable to other experimental values reported for LD GCs (190–234 MPa,[1,44–46] 204.75 ± 49.81 MPa [47]).

The activation energies for total conductivity of the glass–ceramic materials are significantly higher than those found for lithium disilicate glass[48,49] and close to value obtained for 100% crystallized lithium disilicate.[50] In general, GCs materials featured low total conductivity (~2×10^{-18} S/cm for GK_0) suggesting a number of practical applications in which this property is relevant.

5. Conclusions

The data gathered and discussed in the frame of the present work enable the following conclusions to be drawn:

(1) The sintering/densification of the glass powder compacts occurred in two steps. Sintering started at ~484–491 °C (T_{FS1}) in all compositions whilst the extent of densification along the first stage significantly decreased with increasing the added amounts of K_2O and the K_2O/SiO_2 ratio. The second stage of densification occurred in competition with crystallization process.

(2) Increasing the K_2O/SiO_2 ratio led the thermal parameters T_{FS1}, T_{MS1}, T_{FS2} and T_{MS2} to decrease, a trend that was also observed for the temperature intervals between T_{MS} and T_{FS}. This suggests that K_2O-richer samples ($GK_{2.5}$, GK_5 and GK_{10}) get sintered within a shorter temperature interval and at lower temperatures.

(3) The gradual substitution of SiO_2 by K_2O in glass compositions suppressed the crystallization of $Li_2Si_2O_5$ and promoted the formation of Li_2SiO_3 upon sintering the glass powder compacts.

(4) The glass powder compacts demonstrate wider range of the lithium disilicate formation with $x \leq 2$ (≤4.63 mol% K_2O) than the corresponding bulk glasses with $x \leq 1$ (≤3.63 mol% K_2O).

(5) The predominant crystallization of lithium disilicate in low-K_2O compositions resulted in glass–ceramics with high mechanical strength (~173–224 MPa), chemical resistance (~25–50 μg/cm^2) and low total conductivity (~2×10^{-18} S/cm for GK_0) making the materials suitable for a number of practical applications.

Acknowledgements

Financial support from CICECO, University of Aveiro, and from the FCT, Portugal (grant SFRH/BD/41307/2007 and project PTDC/CTM-CER/114209/2009) are gratefully acknowledged.

References

1. Höland W, Beall G. *Glass–ceramic technology*. Westerville, OH: The American Ceramic Society; 2002.
2. Lira C, d Oliveira APN, Alarcon OE. Sintering and crystallisation of $CaO–Al_2O_3–SiO_2$ glass powder compacts. *Glass Technol* 2001;**42**(3):91–6.
3. Boccaccini AR, Schawohl J, Hern H, Schunck B, Rincon JM, Romero M. Sintered glass–ceramics from municipal incinerator fly ash. *Glass Technol* 2000;**41**(3):99–105.
4. Fan CL, Rahaman MN. Factors controlling the sintering of ceramic particulate composites I: conventional processing. *J Am Ceram Soc* 1992;**75**(8):2056–65.
5. Siligardi C, D'Arrigo MC, Leonelli C. Sintering behavior of glass–ceramic frits. *Am Ceram Soc Bull* 2000;**79**(9):88–92.
6. Toya T, Kameshima Y, Yasumori A, Okada K. Preparation and properties of glass–ceramics from wastes (Kira) of silica sand and kaolin clay refining. *J Eur Ceram Soc* 2004;**24**(8):2367–72.
7. Toya T, Tamura Y, Kameshima Y, Okada K. Preparation and properties of $CaO–MgO–Al_2O_3–SiO_2$ glass–ceramics from kaolin clay refining waste (Kira) and dolomite. *Ceram Int* 2004;**30**(6):983–9.
8. Arnault L, Gerland M, Riviere A. Microstructural study of two LAS-type glass–ceramics and their parent glass. *J Mater Sci* 2000;**35**(9):2331–45.
9. Barbieri L, Leonelli C, Manfredini T, Siligardi C, Corradi AB. Nucleation and crystallization of a lithium aluminosilicate glass. *J Am Ceram Soc* 1997;**80**(12):3077–83.
10. Riello P, Canton P, Comelato N, Polizzi S, Verita M, Fagherazzi G, Hofmeister H, Hopfe S. Nucleation and crystallization behavior of glass–ceramic materials in the $Li_2O–Al_2O_3–SiO_2$ system of interest for their transparency properties. *J Non-Cryst Solids* 2001;**288**(1–3):127–39.

11. Kuzielova E, Palou M, Kozankova J. Crystallization mechanism and bioactivity of lithium disilicate glasses in relation to CaO, P_2O_5, CaF_2 addition. *Ceram Silik* 2007;**51**(3):136–41.
12. Lynch ME, Folz DC, Clark DE. Effect of microwaves on the migration of lithium and silicon from lithium disilicate (Li_2O–$2SiO_2$) glass. *Food Addit Contam* 2008;**25**(4):519–26.
13. Wen G, Zheng X, Song L. Effects of P_2O_5 and sintering temperature on microstructure and mechanical properties of lithium disilicate glass–ceramics. *Acta Mater* 2007;**55**(10):3583–91.
14. Schweiger M, Höland W, Frank M, Drescher H, Rheinberger V. IPS Empress 2: a new pressable high-strength glass–ceramic for esthetic all-ceramic restoration. *Quintessence Dent Technol* 1999;**24**(7):876–82.
15. Burgner LL, Lucas P, Weinberg MC, Soares PC, Zanotto ED. On the persistence of metastable crystal phases in lithium disilicate glass. *J Non-Cryst Solids* 2000;**274**(1-3):188–94.
16. Freiman SW, Hench LL. Kinetics of crystallization in Li_2O–SiO_2 glasses. *J Am Ceram Soc* 1968;**51**(7):382–7.
17. Ray CS, Huang WH, Day DE. Crystallization kinetics of a lithia–silica glass: effect of sample characteristics and thermal analysis measurement techniques. *J Am Ceram Soc* 1991;**74**(1):60–6.
18. Soares PC, Zanotto ED, Fokin VM, Jain H. TEM and XRD study of early crystallization of lithium disilicate glasses. *J Non-Cryst Solids* 2003;**331**(1-3):217–27.
19. Fernandes HR, Tulyaganov DU, Goel A, Ribeiro MJ, Pascual MJ, Ferreira JMF. Effect of Al_2O_3 and K_2O content on structure, properties and devitrification of glasses in the Li_2O–SiO_2 system. *J Eur Ceram Soc* 2010;**30**(10):2017–30.
20. Fernandes HR, Tulyaganov DU, Goel IK, Ferreira JMF. Crystallization process and some properties of Li_2O–SiO_2 glass–ceramics doped with Al_2O_3 and K_2O. *J Am Ceram Soc* 2008;**91**(11):3698–703.
21. Fernandes HR, Tulyaganov DU, Goel A, Ferreira JMF. Effect of K_2O on structure-property relationships and phase transformations in Li_2O–SiO_2 glasses. *J Eur Ceram Soc* 2012;**32**(2):291–8.
22. Pascual MJ, Duran A, Prado MO. A new method for determining fixed viscosity points of glasses. *Phys Chem Glasses* 2005;**46**(5):512–20.
23. Pascual MJ, Pascual L, Duran A. Determination of the viscosity–temperature curve for glasses on the basis of fixed viscosity points determined by hot stage microscopy. *Phys Chem Glasses* 2001;**42**(1):61–6.
24. ISO 6872. *International standards for dental ceramics*. Geneva, Switzerland: International Organization for Standardization; 1995.
25. Abdurakhmanov K, Éminov AM, Maslennikova GN. Stages of ceramic structure formation in the presence of additives. *Glass Ceram* 2000;**57**(9–10):354–6.
26. Bernardin AM, de Medeiros DS, Riella HC. Pyroplasticity in porcelain tiles. *Mater Sci Eng A* 2006;**427**:316–9.
27. Liu H, Lu H, Chen D, Wang H, Xu H, Zhang R. Preparation and properties of glass–ceramics derived from blast-furnace slag by a ceramic-sintering process. *Ceram Int* 2009;**35**:3181–4.
28. Pranckeviciene J, Balkevicius V, Spokauskas AA. Investigations on properties of sintered ceramics out of low-melting illite clay and additive of fine-dispersed nepheline syenite. *Mater Sci* 2010;**16**(3):231–5.
29. Torres P, Fernandes HR, Olhero S, Ferreira JMF. Incorporation of wastes from granite rock cutting and polishing industries to produce roof tiles. *J Eur Ceram Soc* 2009;**29**:23–30.
30. Frenkel J. Viscous flow of crystalline bodies under the action of surface tension. *J Phys (USSR)* 1945;**9**:385–91.
31. Prado MO, Zanotto ED, Muller R. Model for sintering polydispersed glass particles. *J Non-Cryst Solids* 2001;**279**(2-3):169–78.
32. Mackenzie JK, Shuttleworth R. A phenomenological theory of sintering. *Proc Phys Soc B* 1949;**62**(12):833–52.
33. Lara C, Pascual MJ, Duran A. Glass-forming ability, sinterability and thermal properties in the systems RO–BaO–SiO_2 (R = Mg Zn). *J Non-Cryst Solids* 2004;**348**:149–55.
34. Scholze H. Influence of viscosity and surface tension on hot stage microscopy measurements on glasses. *Ver Dtsch Keram Ges* 1962;**391**: 63–8.
35. Apel E, van't Hoen C, Rheinberger V, Holand W. Influence of ZrO_2 on the crystallization and properties of lithium disilicate glass–ceramics derived from a multi-component system. *J Eur Ceram Soc* 2007;**27**:1571–7.
36. Bischoff C, Eckert H, Apel E, Rheinberger VM, Holand W. Phase evolution in lithium disilicate glass–ceramics based on non-stoichiometric compositions of a multi-component system: structural studies by ^{29}Si single and double resonance solid state NMR. *Phys Chem Chem Phys* 2011;**13**:4540–51.
37. Strnad Z. *Glass–ceramic materials*. Amsterdam: Elsevier; 1986.
38. Pisciella P, Pelino M. Thermal expansion investigation of iron rich glass–ceramic. *J Eur Ceram Soc* 2008;**28**:3021–6.
39. Volf MB. *Mathematical approach to glass*. Amsterdam: Elsevier; 1988.
40. Xiao Z, Zhou J, Wang Y, Luo M. Microstructure and properties of Li_2O–Al_2O_3–SiO_2–P_2O_5 glass–ceramics. *Open Mater Sci J* 2011;**5**:45–50.
41. Borrelli, N. F., Goetschius, K. L., Morse, D. L., Smith, and C. M., Corning incorporated, Corning, NY, US 7829489, 2010.
42. Höland W, Apel E, van Hoen C, Rheinberger V. Studies of crystal phase formations in high-strength lithium disilicate glass–ceramics. *J Non-Cryst Solids* 2006;**352**(38-39):4041–50.
43. Schweiger, M., Frank, M., Rheinberger, V., and Höland, W. 6,342,458, 1999 (Ivoclar AG).
44. Beall G. Design of glass–ceramics. *Solid State Sci* 1989;**3**:333–54.
45. Beall G. Glass–ceramics: recent developments and application. *Ceram Trans* 1993;**30**:241–66.
46. Echevería LM. New lithium disilicate glass–ceramics. *Boletin da la Sociedad Espanola de Cerámica e Vidrio* 1992;**5**:183–8.
47. Drummond JL, King TJ, Bapna MS, Koperski RD. Mechanical property evaluation of pressable restorative ceramics. *Dental Mater* 2000;**16**(3):226–33.
48. Hench LL, Frieman SW, Kinser DL. Early stages of crystallization in a Li_2O–$2SiO_2$ glass. *Phys Chem Glasses* 1971;**12**(2):58–63.
49. Kone A, Ribes M, Souquet JL. The structure of glasses in the SiO_2–Li_2O–Li_2SiO_4 system studied by means of electrical measurement. *Phys Chem Glasses* 1982;**23**(1):18–22.
50. Campos-Junior AA, Rodrigues ACM. Ionic blocking effect in partially crystallized lithium disilicate. *J Appl Phys* 2006;**100**:053709.